IEEE Robotics and Automation Letters (RA-L) paper, presented at ICRA 2026, Vienna, Austria. Cite as RA-L paper.

Dual Arm Steering of Flexible Linear Objects in 2-D and 3-D Environments Using Euler's Elastica Solutions

A. Levin[1], I. Grinberg[1], E. D. Rimon[1], and A. Shapiro[2]

***Abstract*— This paper describes a method for steering flexible linear objects using two robot hands in environments populated by sparsely spaced obstacles. The approach involves manipulating an elastic inextensible rod by varying the gripping endpoint positions and tangents. Closed form solutions that describe the flexible linear object shape in planar environments, Euler's elastica, are described. The paper uses the elastica solutions to formulate criteria for non self-intersection, stability and obstacle avoidance in analytic closed form manner. These criteria are formulated as constraints in the flexible object six-dimensional configuration space that represents the robot gripping endpoint positions and tangents. In particular, this paper introduces a novel criterion that ensures the flexible object stability during steering. All safety criteria are integrated into a scheme for steering flexible linear objects in planar environments, which is lifted into a steering scheme in three-dimensional environments populated by sparsely spaced obstacles. Experiments with a dual-arm robot demonstrate the method.**

I. Introduction

Robotic manipulation of flexible linear objects is challenging due to their multiple degrees of freedom and the need to account for their self-intersection and stability. Robotic applications include cable routing and untangling [1]–[3], surgical suturing [4], [5], knot tying [6], [7], compliant mechanisms [8] and agricultural robotics [9]. DARPA's Plug-Task challenge [10], EU IntelliMan [11], EU SoftEnable [12] and ICRA workshops [13]–[15] are all dedicated to robotic handling and manipulation of soft and deformable objects. This paper is specifically motivated by the need for robot assisted fresh food handling [16], where flexible linear objects are used to model strip like fresh food items [12].

This paper considers dual arm steering of flexible linear objects in a stable and non self-intersecting manner while avoiding sparsely spaced obstacles (Fig. 1). This paper models flexible linear objects as inextensible elastic rods of various cross-sections, termed *flexible cables*. The paper describes a dual arm steering scheme based on closed-form Euler's elastica solutions in two-dimensions, which have been widely validated in the solid mechanics literature [17], [18]. The paper then demonstrates how the 2-D steering scheme can be lifted into a dual arm steering scheme in three-dimensional environments populated by sparsely spaced obstacles. The paper assumes the cable elastic energy dominates then the cable gravitational energy. Thus, 3-D flexible cable manipulation can be achieved without significant gravitational effects (Fig. 1).

Fig. 1: A dual-arm robot has to steer a flexible linear object in a stable and non self-intersecting manner while avoiding sparsely spaced obstacles.

Related work: When a flexible cable is subjected to endpoint forces and moments that maintain its equilibrium state in the plane, its curvature at each point is proportional to the *bending moment* at this point according to Euler-Bernoulli bending moment law. See Wakamatsu [19] for a survey of flexible linear object modeling techniques.

In the robotics literature, sampling-based approaches are used to plan flexible cables steering paths. Moll [20] samples cable endpoint positions, then computes their stable shapes by numerical optimization of the flexible cable total elastic energy. Bretl [21] uses Sachkov's theory to describe the flexible cable total elastic energy minimization as an optimal control problem. Bretl shows that the *adjoint equation* which describes the flexible cable equilibrium shapes when held by two robot hands is fully determined by a small number of costate variables. In 2-D environments, these are endpoint forces and moments (three variables), while in 3-D environments these are endpoint forces and torques (six variables). Bretl [21] used this insight to design sample-based planners that steer flexible cables in 2-D and 3-D settings. However, in order to verify the *stability* of each sampled flexible cable shape, the costate-to-endpoint Jacobian must be computed by solving the *conjugate differential equation*. Sintov [22] built upon this work by introducing a two-stage process. First generating stable flexible cable shapes for sampled costates, then determining the cable steering path using numerical tests for self-intersection and obstacle avoidance. Yu [23] models

This work receives funding from the European Union's research and innovation program under grant no. 101070600, project SoftEnable.

[1] Aharon Levin, aharon.levin@campus.technion.ac.il,ORCID:0009-0006-9068-7011, Itay Grinberg, itaygrinberg@campus.technion.ac.il,ORCID:0009-0000-0932-9433 , Elon Rimon, rimon@me.technion.ac.il ORCID:0000-0002-8270-6167 . Dept. of ME, Technion, Israel, . [2] Amir Shapiro, ashapiro@bgu.ac.il ORCID: . Dept. of ME, Ben-Gurion University, Israel.

flexible linear objects as spring-mass systems whose shape is parametrized by m equally spaced features. A steering path is computed by sampling $\mathbb{R}^{3m}$ and projecting each sample to a minimum energy shape of the spring-mass system. A local MPC feedback controller then steers the flexible cable along the planned path. The current paper offers a different approach for steering flexible linear objects using Euler's elastica parameters that fully predict the objects stable and non-intersecting shapes in analytic closed form manner.

Paper contributions: This paper steering scheme is based on Euler's elastica solutions for flexible cables equilibrium shapes when held by two robot hands in two-dimensions. The flexible cable *configuration space* consists of its base-frame position and orientation (three variables), and three elastica shape parameters. In previous work [24], we considered flexible cable steering in planar environments using equal endpoint tangents defined by specific planar cells of the flexible cable elastica parameters. These are cells $1, \ldots, 4$ in Fig. 2(a). This paper considers the *three-dimensional* elastica parameter space shown in Fig. 2(b), where the flexible cable is held with arbitrary endpoint positions and tangents during steering. This generalization is achieved by a novel geometric rule that ensures the flexible cable stability during steering.

The flexible cable stability and non self-intersection are formulated as constraints in the elastica parameter space. The paper then describes a piecewise convex representation of the flexible cable equilibrium shapes that is used to efficiently check collision with obstacles during steering. All of these tools are incorporated into a dual arm steering scheme in planar environments. The paper then demonstrates with experiments how the planar scheme can be used to steer flexible cables in 3-D environments populated by sparsely spaced obstacles. This scenario is referred to as *semi-spatial,* since the flexible cable deformation is confined to a plane which is free to rotate and translate in 3-D space. The paper thus highlights the availability of *a 9-D submanifold* (base frame position and orientation and three elastica parameters) embedded in the flexible cable 12-D configuration space, that used to steer flexible cables in 3-D space using Euler's elastica solutions.

The paper is organized as follows. Section II summarizes the elastica solutions for flexible cable equilibrium shapes and the flexible cable configuration space. Section III describes a subset of the flexible cable configuration space that ensures non self-intersection and stability during steering. Section IV describes an efficient collision detection technique, then integrates all tools into a dual arm steering scheme. Section V describes experiments of the steering scheme in 2-D and 3-D obstacle environments. The conclusion suggests future research topics. Two appendices contain proof details and a criterion for neglecting gravity during 3-D steering.

II. Flexible Cable Mechanics

This section describes the elastica solutions for flexible cable equilibrium shapes, the elastica shape parameters, then the configuration space associated with these parameters.

Euler's elastica solutions: The flexible cable equilibrium shapes are obtained by solving an optimal control problem

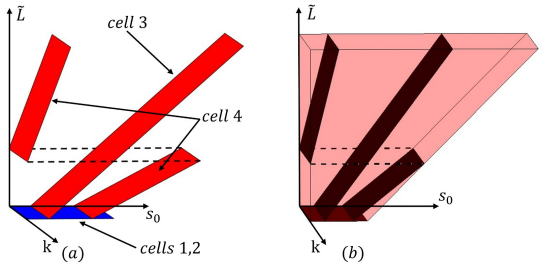

Fig. 2: The flexible cable elastica parameters describe its equilibrium shapes. (a) Previous work focused on flexible cable held with equal endpoint tangents. (b) This paper considers the full range of elastica parameters where the flexible cable is steered with arbitrary endpoint positions and tangents.

[21]. In two-dimensions, we assume an inextensible flexible cable of length L parameterized by $(x(s), y(s))$ for $s \in [0, L]$. The cable's *state variables* are its $(x(s), y(s))$ coordinates and its tangent direction $\phi(s)$, forming the state vector $S = (x, y, \phi)$. The curvature of the cable under arc-length parametrization is $\kappa(s) = \frac{d}{ds}\phi(s)$, which serves as a continuous piecewise smooth *control input,* $u(s) = \kappa(s)$, for the flexible cable system equations

$$\tfrac{d}{ds}S(s) = \begin{pmatrix} \dot{x}(s) \\ \dot{y}(s) \\ \dot{\phi}(s) \end{pmatrix} = \begin{pmatrix} \cos\phi(s) \\ \sin\phi(s) \\ u(s) \end{pmatrix} \qquad s \in [0, L]. \tag{1}$$

The flexible cable shape, parameterized by arclength in Eq. (1), is determined by its curvature as control input. When the flexible cable is modeled as an inextensible elastic rod in a planar environment, its total elastic energy is given by

$$J = \tfrac{1}{2}EI \cdot \int_0^L \kappa^2(s) ds \tag{2}$$

where $E > 0$ is Young's modulus of elasticity and $I > 0$ is the cable cross-sectional second moment of inertia [26]. The cable stiffness, EI, is a known parameter.

When two robot hands grasp a flexible cable at fixed endpoint positions and tangents, $S(0) = (x(0), y(0), \phi(0))$ and $S(L) = (x(L), y(L), \phi(L))$, the flexible cable locally stable shapes form *local minima* of J, subject to the endpoint constraints and the cable fixed length constraint described by Eq. (1). As J represents bending energy that increases continuously with increasing cable curvature (until reaching plastic yield limit), there always exist stable cable shapes that satisfy the fixed endpoint positions and tangents. The *normal Hamiltonian* [25] (the abnormal case is related to straight line shape [21]) of the cable system defined by Eq. (1) and the elastic energy J is given by

$$H(S, \boldsymbol{\lambda}, u) = \lambda_x \cdot \cos\phi + \lambda_y \cdot \sin\phi + \lambda_\phi u + \tfrac{1}{2}EI \cdot u^2 \tag{3}$$

where $\boldsymbol{\lambda}(s) = (\lambda_x(s), \lambda_y(s), \lambda_\phi(s))$ are the *costate variables.* The costates λ_x, λ_y, and λ_ϕ correspond to internal force and bending moment along the flexible cable. The equilibrium states of the cable when held by two robot hands are energy extremal cable shapes. The *adjoint equation* [26] can be used to determine the costate vector $\boldsymbol{\lambda}(s)$ along an extremal shape

$$\frac{d}{ds}\boldsymbol{\lambda}(s) = -\nabla_S H(S, \boldsymbol{\lambda}, u) \qquad S = (x, y, \phi)$$

thus leading to the system of adjoint differential equations

$$\dot{\lambda}_x = 0, \dot{\lambda}_y = 0, \dot{\lambda}_\phi(s) = \lambda_x(s) \cdot \sin\phi(s) - \lambda_y(s) \cdot \cos\phi(s) \tag{4}$$

while the control $u(s) = \kappa(s)$ satisfies an additional condition

$$\tfrac{\partial H}{\partial u} = 0$$

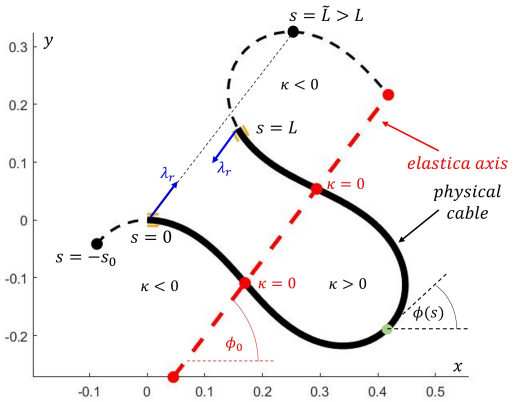

Fig. 3: Top view of a full period elastica shape with the physical flexible cable of length L embedded in its periodic elastica solution of period length $\tilde{L}$. The elastica axis with angle ϕ_0 passes through the zero curvature points and is parallel to the opposing forces of magnitude λ_r applied at the flexible cable endpoints (blue arrows).

thus leading to the algebraic equation

$$\lambda_\phi(s) + EI \cdot u(s) = 0 \tag{5}$$

which is Euler-Bernoulli bending moment law. Using Eq. (4), $\lambda_x(s)$ and $\lambda_y(s)$ are constant along energy extremal cable shapes. These constants define the costate parameters λ_r and ϕ_0

$$\begin{pmatrix}\lambda_x\\ \lambda_y\end{pmatrix} = \lambda_r \cdot \begin{pmatrix}\cos\phi_0\\ \sin\phi_0\end{pmatrix}, \quad \lambda_r = \sqrt{\lambda_x^2 + \lambda_y^2}$$

where λ_r is the magnitude and ϕ_0 the direction of the forces applied at the flexible cable endpoints (blue arrows in Fig. 3). As the system defined by Eq. (1) is autonomous with no explicit dependence on s, the Hamiltonian remains constant along energy extremal cable shapes, $H(s) = H^*$ for $s \in [0, L]$. Substituting $\lambda_\phi(s) = -EI \cdot u(s)$ from Eq. (5) into $H(s)$ and replacing $u(s)$ by $\kappa(s)$ gives

$$\lambda_r(\cos\phi(s)\cos\phi_0 + \sin\phi(s)\sin\phi_0) - \tfrac{1}{2}EI\cdot\kappa^2(s) = H^* \tag{6}$$

Taking the derivative of both sides w.r.t. s gives

$$\lambda_r(-\sin\phi(s)\cos\phi_0 + \cos\phi(s)\sin\phi_0) - EI\cdot\frac{d}{ds}\kappa(s) = 0 \tag{7}$$

where we canceled the common factor $\kappa(s) = \frac{d}{ds}\phi(s)$. Substituting the system equations $\dot{x}(s) = \cos\phi(s)$ and $\dot{y}(s) = \sin\phi(s)$ into Eqs. (6) and (7) gives

$$\lambda_r \cdot R(\phi_0) \cdot \begin{pmatrix}\dot{x}(s)\\ \dot{y}(s)\end{pmatrix} = \begin{pmatrix}\frac{1}{2}EI\cdot\kappa^2(s) + H^*\\ EI\cdot\frac{d}{ds}\kappa(s)\end{pmatrix}$$

where $R(\phi_0) = \begin{bmatrix}\cos\phi_0 & \sin\phi_0\\ \sin\phi_0 & -\cos\phi_0\end{bmatrix}$. Integrating both sides, $\int_0^s \dot{x}(t)dt$ and $\int_0^s \dot{y}(t)dt$, gives the flexible cable (x,y) coordinates in terms of its curvature

$$\begin{pmatrix}x(s)\\ y(s)\end{pmatrix} = \begin{pmatrix}x(0)\\ y(0)\end{pmatrix} + \frac{1}{\lambda_r}R(\phi_0)\cdot\begin{pmatrix}\frac{1}{2}EI\cdot\int_0^s\kappa^2(t)dt + H^*\cdot s\\ EI\cdot(\kappa(s) - \kappa(0))\end{pmatrix}$$

where $s \in [0, L]$. This paper focuses on flexible cable equilibrium shapes that exhibit inflection points, known as *inflectional elastica* (Fig. 3). The curvature of the inflectional elastica is described by an *elliptic cosine function,* $\mathrm{cn}(\cdot,\cdot)$, of the cable path length parameter [17][p. 402-404]

$$\kappa(s) = -2k\sqrt{\lambda}\cdot\mathrm{cn}(\sqrt{\lambda}\cdot(s+s_0), \mathrm{k}) \qquad s \in [0, L] \tag{8}$$

where the *elliptic modulus parameter,* $0 \le \mathrm{k} < 1$, is discussed below and $\lambda = \frac{\lambda_r}{EI}$. The elliptic cosine function is periodic, similar to the cosine function, and has two zeros per period [27]. To get the cable shape, one integrates Eq. (8):

$$\begin{pmatrix}x(s)\\ y(s)\end{pmatrix} = \begin{pmatrix}x(0)\\ y(0)\end{pmatrix} + R(\phi_0)\cdot\begin{pmatrix}\tilde{x}(s)\\ \tilde{y}(s)\end{pmatrix} \tag{9}$$

where

$$\begin{pmatrix}\tilde{x}(s)\\ \tilde{y}(s)\end{pmatrix} = \begin{pmatrix}\frac{2}{\sqrt{\lambda}}\left(\epsilon(\sqrt{\lambda}(s+s_0), \mathrm{k}) - \epsilon(\sqrt{\lambda}\cdot s_0, \mathrm{k})\right) - s\\ -\frac{2\mathrm{k}}{\sqrt{\lambda}}\left(\mathrm{cn}(\sqrt{\lambda}(s+s_0), \mathrm{k}) - \mathrm{cn}(\sqrt{\lambda}\cdot s_0, \mathrm{k})\right)\end{pmatrix}$$

where $\epsilon(\cdot,\cdot) = E(\mathrm{am}(\cdot,\cdot),\cdot)$, $\mathrm{am}(\cdot,\cdot)$ is *Jacobi amplitude function* and $E(\cdot,\cdot)$ is *incomplete second kind elliptic integral* [27].

Flexible cable shape parameters: The flexible cable equilibrium shapes can be described by three parameters (Fig. 3). These are the modulus parameter, k, a phase parameter s_0 that measures the physical cable start point and the parameter $\tilde{L}$ that measures the full period length of the elastica solution (Fig. 3). First consider the parameter $\lambda = \frac{\lambda_r}{EI}$ in Eq. (8). The elliptic cosine function period is $4K(\mathrm{k})$, where $K(\mathrm{k})$ is the complete elliptic integral of the first kind.[1] The argument $\sqrt{\lambda}(s+s_0)$ in Eq. (8) satisfies the full-period relation $\sqrt{\lambda}\cdot\tilde{L} = 4\cdot K(\mathrm{k})$, which gives

$$\lambda(\mathrm{k}, \tilde{L}) = (4K(\mathrm{k})/\tilde{L})^2 \tag{10}$$

Next consider the parameter H^* in Eq. (6). Since $H(s) = H^*$ for $s \in [0, L]$, the value of H^* can be determined at any point along the cable length. At the zero curvature points, $\kappa(s^*) = 0$, Eq. (6) gives $H^*(\mathrm{k}, \tilde{L}) = \lambda_r\cdot(\cos\phi(s^*)\cos\phi_0 + \sin\phi(s^*)\sin\phi_0) = EI\cdot\lambda(\mathrm{k}, \tilde{L})\sigma(\mathrm{k})$, where $\phi_0 = \phi(0) + 2\sin^{-1}(\mathrm{k}\cdot\mathrm{sn}(\sqrt{\lambda}s_0, \mathrm{k}))$ and $\sigma(\mathrm{k}) = \cos(\phi(s^*) - \phi_0) = 1 - 2\mathrm{k}^2$, Additionally, [24] shows that the flexible cable tangent, $\phi(s)$, is given in terms of an *elliptic sine function,* $\mathrm{sn}(\cdot,\cdot)$, by

$$\phi(s) = \phi_0 - 2\sin^{-1}\left(\mathrm{k}\cdot\mathrm{sn}\sqrt{\lambda}(s+s_0), \mathrm{k}\right) \quad s \in [0, L]. \tag{11}$$

The flexible cable equilibrium shapes are thus determined by *six parameters*: the cable base frame position and orientation, $(x(0), y(0), \phi(0))$, and the elastica parameters $(\mathrm{k}, s_0, \tilde{L})$.

Flexible cable configuration space: The flexible cable shape is fully determined by its base frame position and tangent and the elastica parameters using Eq. (9). The flexible cable steering path between start and target shapes can be planned in the six-dimensional configuration space defined as $\mathcal{C} = \{S(0) \times (\mathrm{k}, s_0, \tilde{L}) \in \mathbb{R}^3 \times \mathbb{R}^3\}$, which measures the flexible cable base frame position and orientation, then the modulus, phase and full-period length elastica parameters. The dual arms *feasible gripping states* (endpoint positions and tangents) under inextensible flexible cable constraint is

$$\Delta = \left\{(S(0), S(L)) \in \mathbb{R}^3 \times \mathbb{R}^3 : \left\|\begin{pmatrix}x(L)\\ y(L)\end{pmatrix} - \begin{pmatrix}x(0)\\ y(0)\end{pmatrix}\right\| \le L\right\}.$$

The flexible cable steering scheme will use the map $\psi : \mathcal{C} \to \Delta$, which maps configuration space points, $q = (x(0), y(0), \phi(0), \mathrm{k}, s_0, \tilde{L})$, to feasible gripping states, $\psi(q) = (x(0), y(0), \phi(0), x(L), y(L), \phi(L))$, see Fig. 4 for a simplified illustration showing Δ at $S(0) = 0$. The steering scheme will plan the flexible cable path in $\mathcal{C}$ and use ψ to map points of $\mathcal{C}$ to dual arm gripping endpoints and tangents.

In 3-D workspace, the flexible cable deformation remains planar while the deformation plane is free to rotate and translate by a 3-D rigid body transformation. Thus, Eq. (9) becomes

[1] It is defined as $K(\mathrm{k}) = \int_0^{\frac{\pi}{2}} \frac{d\theta}{\sqrt{1-\mathrm{k}^2 sin^2\theta}}$, a standard analytic function of the modulus parameter k [27].

$$\begin{pmatrix} x(s) \\ y(s) \\ z(s) \end{pmatrix} = \begin{pmatrix} x(0) \\ y(0) \\ z(0) \end{pmatrix} + R_x(\phi_x)R_y(\phi_y)R(\phi_0)\cdot \begin{pmatrix} \tilde{x}(s) \\ \tilde{y}(s) \\ 0 \end{pmatrix} \quad (12)$$

where $R(\phi) = \begin{bmatrix} \cos\phi_0 & \sin\phi_0 & 0 \\ \sin\phi_0 & -\cos\phi_0 & 0 \\ 0 & 0 & 1 \end{bmatrix}$ while R_x and R_y are rotation matrices around the world frame x and y axes. In the 3-D case, the flexible cable configuration space is defined by $\mathcal{C} = \mathbb{R}^3 \times SO(3) \times \mathbb{R}^3$, and points in $\mathcal{C}$ are $q = (x(0), y(0), z(0), \phi_x, \phi_y, \phi(0), \mathrm{k}, s_0, \tilde{L})$ where $\phi(0)$ is the tangent direction within the flexible cable deformation plane. Appendix B describes under what conditions the flexible cable elastic energy dominates its gravitational energy.

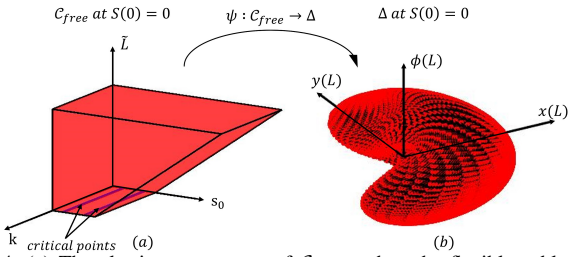

Fig. 4: (a) The elastica parameters of $\mathcal{C}_{free}$ when the flexible cable base frame is fixed at the origin, $S(0) = 0$. (b) Flexible cable distal endpoint, $(x(L), y(L), \phi(L)) = \psi(q)$ for $q \in \mathcal{C}_{free}$ with $S(0) = 0$. Purple lines on bottom of (a) are elastica shapes at which $L = \tilde{L}$ while $s_0 = \frac{L}{4}$ or $s_0 = \frac{3L}{4}$. $\mathcal{C}_{free} \subset \mathcal{C}$ is explained in Section III.

III. The Safe Configuration Space

This section characterizes the set of elastica parameters that ensure stability and non self-intersection of the flexible cable equilibrium shapes in two-dimensions.

Stable configuration space: The flexible cable local stability ensures robustness of its shape under small gripper manipulation errors and robot arm disturbances (see video clips attached to submission). Moreover, a flexible cable that continuously maintains local stability is prevented from snapping into nearby local minima during manipulation, a phenomenon known as *snap-buckling* [28]. Based on [29][theorem 28.1] expressed with optimal control formulation, a necessary and sufficient condition for the flexible cable local stability is given by three conditions that must be satisfied simultaneously.

Theorem 1 [local stability]: *When the following conditions are satisfied, the flexible cable shape forms a local minimum of J or equivalently* **a locally stable** *equilibrium shape*

1) *The triplet $(S, \boldsymbol{\lambda}, u)$ must satisfy the flexible cable system and adjoint equations $\dot{S}^* = \nabla_{\boldsymbol{\lambda}} H^*, \dot{\boldsymbol{\lambda}} = -\nabla_S H^*$ (energy extremal flexible cable shape).*
2) *Along the extremum cable shape, $\frac{\partial H}{\partial u} = 0$ and $\frac{\partial^2 H}{\partial u^2} > 0$ (Legendre's necessary condition for a local minimum).*
3) *The flexible cable shape contains no conjugate point in the interval $[0, L]$.*

Where $H(S, \boldsymbol{\lambda}, u)$ is the flexible cable Hamiltonian of Eq. (3).

The next lemma asserts the local stability of *full period* elastica shapes. The lemma uses the critical modulus parameter, $\mathrm{k}_c = 0.908$, at which the elastica full period forms a figure eight shape (Fig. 5(a)).

Lemma 1 [full period stability]: *All full period elastica shapes with $L = \tilde{L}$ and $\mathrm{k} \in [0, \mathrm{k}_c]$ are locally stable, except*

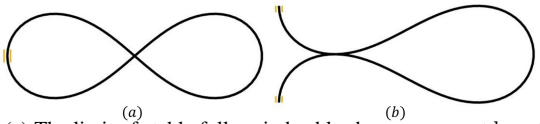

Fig. 5: (a) The limit of stable full-period cable shapes occurs at $\mathrm{k}_c = 0.908$, which forms a figure eight. (b) The limit of non self-intersecting cable shapes occurs at $\mathrm{k}_{max} = 0.855$, at which the full-period elastica just touches itself.

full period shapes having phase parameter $s_0 = \frac{L}{4}$ or $\frac{3L}{4}$.

The proof of Lemma 1 appears in Appendix 1. Lemma 1 is now used to establish the local stability of all sub full-period cable shapes with $L < \tilde{L}$ such that $\mathrm{k} \in [0, \mathrm{k}_c]$.

Theorem 2 [locally stable cable shapes]: *Using flexible cable configuration parameters, $(x(0), y(0), \phi(0), \mathrm{k}, s_0, \tilde{L}) \in \mathbb{R}^6$, the subset of the cable equilibrium shapes given by*

$$\mathcal{C}_{stable} = \big\{(x(0), y(0), \phi(0), \mathrm{k}, s_0, \tilde{L}) \in \mathbb{R}^6 : 0 \le \mathrm{k} < \mathrm{k}_c, \; 0 \le s_0 < \tilde{L}, L \le \tilde{L}, \text{ s.t. at } L = \tilde{L}, s_0 \ne \tfrac{L}{4} \text{ or } \tfrac{3L}{4}\big\} \quad (13)$$

form locally stable flexible cable shapes.

Proof: Consider the three conditions of Theorem 1. One can verify by direct substitution that Euler's elastica form non-trivial solutions $(S, \boldsymbol{\lambda})$ of the adjoint equations (4), as well as solutions of Eqs. (5) and (8) where $u(s) = \kappa(s)$ for $s \in [0, L]$. Hence, according to the first item in Theorem 1, the solution $(S, \boldsymbol{\lambda})$ is an extremum. Next, in the case of flexible cables, $\frac{\partial^2 H}{\partial u^2} = EI > 0$, as required by Legendre's necessary condition. Let us now focus on the third item of Theorem 1, showing that all flexible cable shapes with parameters specified by Eq. (13) have *no conjugate points*.

Consider the local stability of *full-period* elastica shapes, with length $L = \tilde{L}$ such that $\mathrm{k} \in [0, \mathrm{k}_c]$ (Lemma 1). The full-period elastica parameters form *a subset* of the elastica parameters specified by Eq. (13). This subset, $\mathcal{C}_{full-period} \subset \mathcal{C}_{stable}$, consists of elastica parameters $\mathrm{k} \in [0, \mathrm{k}_c]$ and $s_0 \in [0, L]$ such that $L = \tilde{L}$ (physical cable length equals elastica full period length). All other elastica shapes in $\mathcal{C}_{stable}$ form *sub full-period shapes,* with $L < \tilde{L}$. When the physical cable is *shorter* than the elastica full period length, $L < \tilde{L}$, the *principle of optimality* [30][Section 5.1.2] holds for the flexible cable system of Eq. (1). Based on this principle, when the full-period elastica shape that starts at $s = s_0$ and ends at $s = s_0 + \tilde{L}$ is *optimal,* every sub full-period shape that starts at $s = s_0$ and ends at $s = s_0 + L$ such that $L < \tilde{L}$ is also optimal. Hence any sub full-period shape occupied by the physical cable, $s_0 \le s \le s_0 + L$, contains *no conjugate point* to its start point $s = s_0$. Thus, all three conditions of Theorem 1 are satisfied. □

Remark: Theorem 2 is consistent with Sachkov [31][Corollary 3.3] and captures the local stability of the *subset* of flexible cable shapes used in this paper steering scheme.

Non self-intersection configuration space: The non self-intersection condition depends solely on the modulus parameter k [24] as follows. Consider the interval $\mathrm{k} \in [0, \mathrm{k}_{max}]$, where at $\mathrm{k}_{max} = 0.855$ the flexible cable touches itself for the *first time* along the elastica full period shape (Fig. 5(b)). When $0 \le \mathrm{k} \le \mathrm{k}_{max}$, the flexible cable is locally stable and has no self-intersection. This conservative subset of the flexible cable c-space, $\mathcal{C}_{free} \subset \mathcal{C}_{stable}$, is given by

$$\mathcal{C}_{free} = \{(x(0), y(0), \phi(0), \mathrm{k}, s_0, \tilde{L}) \in \mathbb{R}^6 : 0 \le \mathrm{k} < \mathrm{k}_{max}, \; 0 \le s_0 < \tilde{L}, L \le \tilde{L}, \text{ s.t. at } L = \tilde{L}, s_0 \ne \tfrac{L}{4} \text{ or } \tfrac{3L}{4}\}$$

When the flexible cable path is planned in C_{free}, it is kept stable and non self-intersecting.

IV. Cable Steering in Presence of Obstacles

This section describes an efficient collision detection technique for the flexible cable when steered among polygonal obstacles, then describes a scheme that plans the flexible cable steering path in the presence of obstacles.

Algorithm 1 Bounding Triangles Computation

Input: vector $q = (q_1, \ldots, q_6) \in \mathcal{C}_{free}$, cable length L

Initialize($v_0 = (q_1, q_2)$, $\phi_0 = q_3$, $\mathcal{V} = \{v_0\}$, $s^* = \infty$)
if $q_5 < \frac{q_6}{4}$ and $q_5 + L > \frac{q_6}{4}$ **then**
  $s^* \leftarrow \frac{q_6}{4}$
else if $q_5 < \frac{q_6}{2}$ and $q_5 + L > \frac{q_6}{2}$ **then**
  $s^* \leftarrow \frac{q_6}{2}$
else if $q_5 < \frac{3q_6}{4}$ and $q_5 + L > \frac{3q_6}{4}$ **then**
  $s^* \leftarrow \frac{3q_6}{4}$
else if $q_5 < q_6$ and $q_5 + L > q_6$ **then**
  $s^* \leftarrow q_6$
while $q_5 < s^* < q_5 + L$ **do**
  $v_{i+1} \leftarrow (x(s^* - q_5), y(s^* - q_5))$
  $\phi_{i+1} \leftarrow \phi(s^* - q_5)$
  $m_i \leftarrow line(v_i, \phi_i) \cap line(v_{i+1}, \phi_{i+1})$
  $\mathcal{V} \leftarrow V \cup \{m_i, v_{i+1}\}$
  $s^* \leftarrow s^* + \frac{q_6}{4}$
  $i \leftarrow i + 1$
$n \leftarrow i, v_n \leftarrow (x(L), y(L)), \phi_n = \phi(L)$
$m_{n-1} \leftarrow line(v_{n-1}, \phi_{n-1}) \cap line(v_n, \phi_n)$
$\mathcal{V} \leftarrow \mathcal{V} \cup m_{n-1}, v_n$
return $\mathcal{V}$

Output: triangle vertices $\mathcal{V} = \{v_0, m_0, \ldots, m_n, v_n\}$, $n \le 5$.

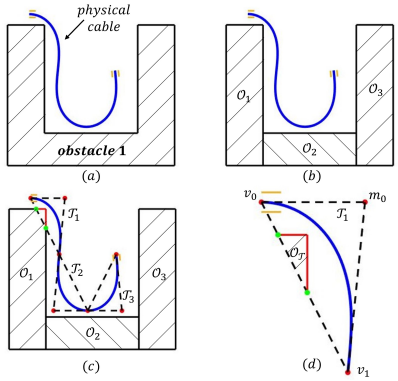

Fig. 6: Collision checker: (a) Physical cable in blue and obstacle in black. (b) Split obstacle into convex pieces O_1, O_2, O_3. (c) Partition the cable to convex arcs then bound arcs by triangles $\mathcal{T}_1, \mathcal{T}_2, \mathcal{T}_3$. Green points are intersection points between $\mathcal{T}_i$-O_j pairs, red lines are $O_\mathcal{T} = O_j \cap \mathcal{T}_i$. (d) Flexible cable arc in $\mathcal{T}_1$ uses to check intersection with convex obstacle piece $O_\mathcal{T}$.

Obstacles collision checker: The collision checker operates in four stages illustrated in Fig. 6. Stage I splits the polygonal obstacles into convex pieces (O_1, O_2, O_3 in Fig. 6(b)). This stage is carried out only once. In Stage II, for a given flexible cable shape determined by specific elastica parameters, the elastica solution is used to split the cable into at most five *convex arcs,* then bound each arc by a triangular region ($\mathcal{T}_1, \mathcal{T}_2, \mathcal{T}_3$ in Fig. 6(c)). The first and third vertices of each triangle, v_i and v_{i+1}, are either one of the cable endpoints, extremum curvature points, or zero curvature inflection points along the flexible cable shape, all known in closed form using the elastica solutions at the base frame $S(0)$. The middle vertex of each triangle, m_i, is located at the intersection of the tangent lines to the flexible cable arc at v_i and v_{i+1} (Fig. 6(c)). The bounding triangles computation is summarized as Algorithm 1.

Stage III checks intersection of the flexible cable bounding triangles against each convex obstacle piece. Stage IV computes the portion of each convex obstacle piece that lies inside the flexible cable bounding triangles (red portion of O_1 in Fig. 6(d)). Stage IV tests for intersection using minimum distance between the cable convex arc inside the triangle and the obstacle boundary in this triangle. The collision checker is summarized as Algorithm 2.

Algorithm 2 Obstacle Collision Checker

Input: the vector $q \in \mathcal{C}_{free}$, cable length L, convex obstacle pieces $Obs = \{O_1, O_2, \ldots, O_m\}$.

1: $check \leftarrow FALSE$
2: $\{\mathcal{T}_1, \ldots, \mathcal{T}_n\} \leftarrow$ GetBoundingTriangle(q, L)
3: **for** $i = 1$ to n **do**
4: **for** $j = 1$ to m **do**
5: $O_\mathcal{T} = O_j \cap int(\mathcal{T}_i)$
6: **if** $O_\mathcal{T} \ne \emptyset$ **then**
7: **if** $O_\mathcal{T} \cap ConvCableArc(\mathcal{T}_i) \ne \emptyset$ **then**
8: **return** $check \leftarrow TRUE$

Details of Lines 2 and 7 in Algorithm 2 have been omitted. In Line 2, each bounding triangle is checked for intersection with obstacles in linear time in the number of obstacle vertices. In Line 7, each convex cable arc is discretized into k equal length linear segments (typically $k = 10$). Each linear segment is then checked for intersection with the individual edges of the obstacle pieces in $O_\mathcal{T}$. The obstacle pieces in $O_\mathcal{T}$ are disjoint and there are at most five convex cable arcs ($n = 3$ in Fig. 6). The entire collision check thus takes $O(kn_{obs})$ time, where n_{obs} is the number of obstacle vertices in the flexible cable bounding triangles $\mathcal{T}_1, \ldots, \mathcal{T}_n$.

Flexible cable steering scheme: The flexible cable steering scheme can use any graph search algorithm. This paper implements a *weighted* A^* algorithm in the flexible cable configuration space. The scheme computes a steering path in a 6-D configuration space for planar steering and a 9-D configuration space for semi-spatial steering. To save storage space, our A^* implementation constructs only a graph embedded in the flexible cable configuration space during steering path computation. For each grid cell $q \in \mathcal{C}_{free}$, its 12 or 18 neighbors describe local increase or decrease in c-space coordinates. Using $q = (x(0), y(0), \phi(0), \mathrm{k}, s_0, \tilde{L})$ the cost function of a node i used by the weighted A^* is given by

$$\mathrm{Cost}(q_i) = (1 - w) \cdot G(q_i, q_{i-1}) + w \cdot h(q_i, q_T) \quad (14)$$

where $G(q_i, q_{i-1}) = ||\psi(q_i) - \psi(q_{i-1})|| + G(q_{i-1})$ such that $||\psi(q_i) - \psi(q_{i-1})||$ is Euclidean norm, while $w \in [0, 1]$ is

a tuning parameter. The function $h(q_i, q_T)$ estimates the distance from q_i to the *target* cable configuration, q_T, measured in terms of minimum robot hands movement by the norm $h(q_i, q_T) = ||\psi(q_i) - \psi(q_T)||$, where $\psi(q)$ is defined in Section II. The tuning parameter in Eq. (14) affects the *greediness* of the search algorithm. When $w = 1$, the A^* algorithm becomes highly greedy with reduced execution times. When $w = 0$, the A^* algorithm becomes Dijkstra's algorithm that opens all neighbors of the current node. In real-world applications execution time is more important than optimality, hence $w = 0.88$ is used in our implementation. The flexible cable steering scheme is summarized as Algorithm 3. The algorithm accepts as input start and target cable shapes $q_S, q_T \in \mathcal{C}_{free}$ and computes the flexible cable path in the presence of obstacles.

Dual arms collision checks: The dual arm collision checks have been omitted from Algorithm 3. In our implementation, each link of the dual arms is surrounded by a cylindrical shell. At each manipulation step, all dual arm links are checked both self-collision and collision with obstacles in the environment.

Algorithm 3 Flexible Cable Steering Scheme

Input: start and target $q_S, q_T \in \mathcal{C}_{free}$, obstacles $O_1, \ldots, O_N$.

Set $open = [q_s], close = [\emptyset]$ split obstacles to convex pieces $\{O_1, O_2, \ldots, O_n\}$ s.t. $n \geq N$.
while $open \neq \emptyset$ **do**
  $q^* \leftarrow Min(Cost(open))$
  if $q^* = T$ **then**
    return $\mathcal{P}_{best} = backpointer(q^*)$ (path from q_S to q_T)
  $close \leftarrow q^*$
  for $q_i \in \mathcal{C}_{free}$ and $q_i \notin close$ and $q_i \in neighbor(q^*)$ **do**
    if $q_i \notin open$ **then**
      if ObstacleCollision($q_i, ConvObs, L$)=FALSE **then**
        $open \leftarrow q_i$
      else
        $close \leftarrow q_i$
    else if $Cost(q_i) < Cost(open(i))$ **then**
      $open(i) = q_i$
return $\mathcal{P}_{best} = \emptyset$ {if no path exist}

Output: path $\mathcal{P}_{best}$ from q_S to q_T.

V. Representative Experiments

To demonstrate the flexible cable steering scheme, we performed two proof-of-concept experiments using the dual arm Baxter robot. The flexible linear object used in the experiments is a plastic zip-tie of length $L = 80$ cm. The steering scheme was implemented using MATLAB R2023a with software library Elfun18 [32] to compute elliptic functions and elliptic integrals. The code ran on Dell OptiPlex 7000 with 16GB RAM and Intel core I7-12700 2.1 GHz CPU. The steering scheme receives as input the base frame position and elastica parameters of the zip-tie start and target positions. The output is the trajectory of the dual arms joint angles.

In the steering experiments, the range of the elastica parameters k and s_0 was defined based on the stable non self-intersecting configuration space $\mathcal{C}_{free}$. The elastica parameter $\tilde{L}$ was constrained to the range $[L, 4L]$, allowing the flexible zip-tie shapes to vary between full and quarter period of the full elastica period. The range of the base frame position and orientation was determined by the Baxter robot workspace. The resolution of the configuration parameters was set as $\Delta x(0) = \Delta y(0) = \Delta z(0) = 0.01$ m, $\Delta\phi(0) = \Delta\phi_x = \Delta\phi_y = 2^\circ$, $\Delta\tilde{L} = 0.03L$, $\Delta s_0 = 0.01L$, $\Delta\sigma = 0.015$, where the elastica parameter σ is defined as $\sigma = 1 - 2\mathrm{k}^2$.

The Baxter robot has seven joints per arm. One difficulty during the experiments was the lack of a readily available inverse kinematics (IK) solver for this robot. In order to analytically solve the robot IK problem, we fixed the third joint of each arm which significantly reduced the robot workspace. During path planning, a check was made to ensure that the zip-tie endpoints lie in the robot workspace [33] by checking for the existence of feasible IK solutions. The robot arms occupy large volumes, hence many IK solutions were excluded in order to prevent inter-arm collision.

The steering scheme proof of concept consists of two experiments. First steering the flexible zip-tie in a planar obstacle environment (Fig. 7). Then steering the flexible zip-tie in a semi-spatial manner, where the zip-tie deformation is carried out in a planar manner without torsion (Fig. 8). In the semi-spatial case, the base frame orientation matrix at $s = 0$ is $R_x(\phi_x) \cdot R_Y(\phi_y) \cdot R(\phi_0)$, and the distal endpoint frame orientation matrix at $s = L$ is $R_x(\phi_x) \cdot R_y(\phi_y) \cdot R(\phi_0 + \phi(L))$.

Figs. 7(a)-(d) show the planar steering of the flexible zip-tie between two rectangular obstacles, with snapshots of the elastica steering path computation shown in Figs. 7(e)-(h). Using weighted A^* described in Section IV, the steering path was computed in the flexible cable 6-D configuration space in 4.5 seconds. However, one should keep in mind that RRT algorithms perform equally well in high dimensional configuration spaces. Hence, we also implemented the bi-directional CBiRRT algorithm [34] on the planar steering problem. When computed over 100 runs for the specified endpoint states, the CBiRRT algorithm mean execution time was reduced to 1.58 seconds with standard deviation of 0.87 seconds.

Figs. 8(a)-(d) show the semi-spatial steering of the flexible zip-tie between two cylindrical obstacles, with snapshots of the elastica steering path computation shown in Figs. 8(e)-(h). The steering path was computed in the flexible cable 9-D configuration space in 8.6 seconds. Again, the CBiRRT algorithm performed better than weighted A^*. When computed over 100 runs for the specified endpoint states, the CBiRRT algorithm mean execution time was only 2.31 seconds with standard deviation of 5.01 seconds. Video clips of the experiments are attached to this paper submission, also available in [35].

VI. Conclusion and Future Work

The paper developed a steering scheme for flexible cables held by two robot hands that control the cable endpoints position and tangents. The flexible cable equilibrium shapes are computed using Euler's elastica solutions. The flexible

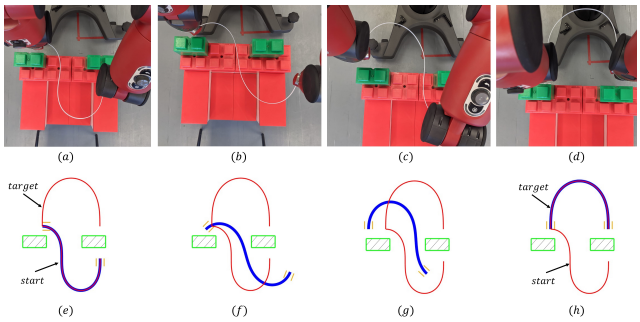

Fig. 7: Flexible cable steering in a planar environment between two obstacles. (a)-(d) Baxter robot snapshots. (e)-(h) Matlab simulation snapshots of the elastica path: red cable is start and target positions, blue cable is current position, green boxes are the obstacles. Note the good fit between the physical zip-tie (upper row) and the elastica prediction shapes (lower row).

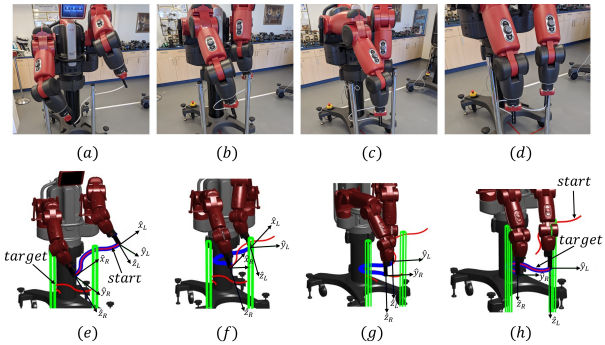

Fig. 8: Flexible cable semi-spatial steering between two cylindrical obstacles. (a)-(d) Baxter robot snapshots. (e)-(h) Matlab simulation snapshots of the elastica path with the dual arm grippers frames overlaid: red cable is start and target positions, blue cable is current position, green cylinders are the obstacles (see video clips attached to submission).

cable configuration space in planar environments consists of the cable base frame position and orientation and the elastica parameters k, s_0 and $\tilde{L}$, forming a 6-D configuration space. The elastica parameters that ensure stability and non self-intersection define the allowed configuration space, $\mathcal{C}_{free}$. To allow flexible cable steering in the presence of obstacles in $\mathcal{C}_{free}$, an efficient technique that checks collision of the flexible cable convex arcs against obstacles was described. These tools were incorporated into a flexible cable steering scheme that was implemented and demonstrated with experiments. First in planar environments then in three-dimensions where the flexible cable maintains planar formations while moving its base-frame freely in a 9-D configuration space.

Future research will extend this work in several ways. First, the range of the elliptic modulus parameter will be extended from $0 \leq \mathrm{k} < \mathrm{k}_{max}$ to any k in the range $[0, 1)$ still without self-intersection. This extension will use an implicit expression that captures the flexible cable's self-intersecting points in terms of the elastica parameters. The second extension will consider flexible cable steering by two robot hands under gravity in two-dimensions. Under gravity, the flexible cable shape minimizes the combined elastic and gravitational potential energies. The third extension will consider flexible cable steering by a *single* robotic hand while the flexible cable distal endpoint is held against a wall or a table. Under such single-hand steering, zero moment constraint holds at the contacting tip or laid segment tip, captured by the co-state condition $\lambda_\phi(L) = 0$. Finally, an important practical extension under progress adapts the flexible cable steering method to close-loop steering control. At each step the global planner computes N forward steps, a single steering step executed, then the true cable shape measured by a camera and used to re-calibrate the global planner for the next N forward steps.

APPENDIX A – PROOF OF LEMMA 1

This appendix explains why full-period elastica shapes are locally stable for all $\mathrm{k} \in [0, \mathrm{k}_c]$.

Auxiliary Lemma [stable equal endpoint tangents]: *When a flexible cable is held with equal endpoint tangents, the flexible cable is*

1) *possibly stable if the cable shape contains one or two inflection point.*
2) *unstable if the cable shape contains three or more inflection points.*

A proof of the auxiliary lemma appears in [24][Corollary 4.1]. Using the auxiliary lemma, three possibly stable shapes with equal endpoint tangents exist: full period elastica with $L = \tilde{L}$, $s_0 \in [0, L]$ and $\mathrm{k} \in [0, 1)$; and less than full period shapes with $L < \tilde{L}$, $\mathrm{k} \in [0, 1)$ and either $s_0 = \tilde{L}/4 + (\tilde{L} - L)/2$ or $s_0 = 3\tilde{L}/4 + (\tilde{L} - L)/2$. The proof of Lemma 1 from Section III follows.

Proof of Lemma 1: Using numerical means shown in Fig. 9, we show that for all the equal endpoint tangent shapes that are possibly stable according to the auxiliary lemma with base frame $S(0) = (0, 0, 0)$, flexible cable shapes in the domain $s_0 \in [0, L], \mathrm{k} \in [0, \mathrm{k}_c]$, and $L = \tilde{L}$ form a global minimum of the flexible cable's total elastic energy. Consider the flexible cable total elastic energy given by $J = \frac{1}{2} EI \cdot \int_0^L \kappa^2(s) ds = 2EI \cdot \sqrt{\lambda} P$ where $P = \epsilon(\sqrt{\lambda}(s_0 + L), \mathrm{k}) - \epsilon(\sqrt{\lambda} s_0, \mathrm{k}) - \sqrt{\lambda}(1 - \mathrm{k}^2) L$ and $\epsilon(f(s), \mathrm{k}) = E(\mathrm{am}(f(s), \mathrm{k}), \mathrm{k})$. Based on Fig. 9(a)-(b), for all full-period shapes with $\mathrm{k} > \mathrm{k}_c$ (green points), there exists another full-period shape with $0 < \mathrm{k} < \mathrm{k}_c$ (blue points) or less than full-period shape (red points) having the same endpoint constraints that has *a lower* total elastic energy J (Fig. 9(a)). Additionally, there is *no overlap* between the J value of full-period shapes with $\mathrm{k} < \mathrm{k}_c$ and shapes with less than full-period. The full-period shapes with $\mathrm{k} < \mathrm{k}_c$ are thus global minima of J that form locally stable shapes (Fig. 9(b)). □

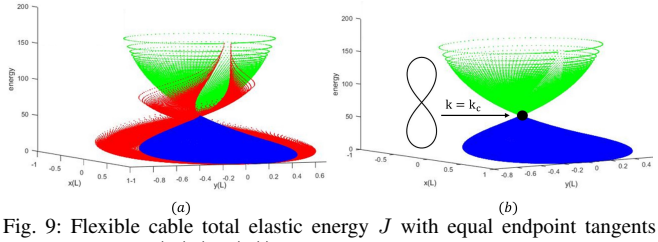

Fig. 9: Flexible cable total elastic energy J with equal endpoint tangents plotted above the $(x(L), y(L))$ plane: (a) Blue points are full-period shapes with $0 \leq \mathrm{k} < \mathrm{k}_c$. Red points are stable equal endpoint tangent shapes with less than a full-period, green points are full-period shapes with $\mathrm{k}_c \leq \mathrm{k} \leq 1$. (b) Blue points are full-period shapes with $0 \leq \mathrm{k} < \mathrm{k}_c$. Green points are full-period shapes with $\mathrm{k}_c \leq \mathrm{k} \leq 1$. The energy-level hourglass surface shows the global minimality of the blue points. Black point between the blue and green points represents the full-period *figure eight* shape with $\mathrm{k} = \mathrm{k}_c$. All blue points represent locally stable full-period shapes.

APPENDIX B – NEGLECTING GRAVITY DURING SEMI-SPATIAL STEERING

This appendix describes a criterion for neglecting the relative effect of gravity during 3-D flexible cable steering. Consider

the three energy functionals: $J_T(S,u) = \int_0^L \left(\frac{1}{2}EI \cdot \kappa^2(s) + \rho g z(s)\right) ds$, $J_E(S,u) = \int_0^L \frac{1}{2}EI \cdot \kappa^2(s) ds$ and $J_G(S,u) = \int_0^L \rho g \cdot z(s) ds$. Here $J_T(S,u)$ is the flexible cable total elastic and gravity energy where ρ is linear mass density, g is the gravitational constant and $z(s)$ is the flexible cable height as a function of its length parameter s. The functional $J_E(S,u)$ represents only the elastic energy stored in the flexible cable while $J_G(S,u)$ represents only the flexible cable gravitational energy.

Using the state variables $S(s) = (x(s), y(s), \phi(s))$ within the current deformation plane, the system $\frac{d}{ds}S(s)$ is still described by Eq. (1) for all three cases. Analytic solutions exist for the flexible cable shapes: (S_E, u_E) the solution that minimizes the functional J_E and (S_G, u_G) the solution that minimizes the functional J_G. Now, the flexible cable total energy can be written as $J_T(S,u) = J_E(S,u) \cdot \left(1 + \frac{J_G(S,u)}{J_E(S,u)}\right)$. When $\frac{J_G(S,u)}{J_E(S,u)} \ll 1$, the flexible cable total energy J_T is dominated by its elastic energy J_E. Furthermore, it holds that $J_G(S_G, u_G) \leq J_G(S,u)$ and $J_E(S_E, u_E) \leq J_E(S,u)$ for all S and u. The ratio $J_G(S_E,u_E)/J_E(S_E,u_E)$ thus forms a *conservative estimate*. When the ratio $\frac{J_G(S_E,u_E)}{J_E(S_E,u_E)} \ll 1$, the effect of gravity can be neglected as illustrated in Fig. 10. Using a flexible zip-tie with linear mass density $\rho = 0.013$ Kg/m and bending stiffness is $EI = 0.0027$ Nm^2 used in Section V, consider the elastica parameters $\mathrm{k} = 0.87367$, $s_0 = 0.13\tilde{L}$ and $\tilde{L} = 1.1L$. For these parameters, $J_G(S_E,u_E)/J_E(S_E,u_E) = 0.0047$ when the zip-tie length is $L = 50$ cm (Fig. 10(a)) while $J_G(S_E,u_E)/J_E(S_E,u_E) = 0.0375$ when the zip-tie length increases to $L = 100$ cm (Fig. 10(b)).

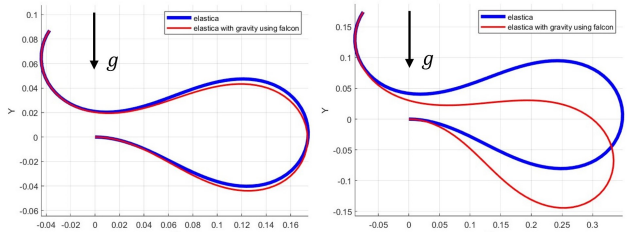

Fig. 10: (a) When $L = 50$ cm, the shape error without gravity is $J_G(S_E,u_E)/J_E(S_E,u_E) = 0.0047$. (b) When $L = 100$ cm for the same parameters, the shape error becomes $J_G(S_E,u_E)/J_E(S_E,u_E) = 0.0375$.

REFERENCES

[1] X. Jiang and coauthors, "Robotized assembly of a wire harness in a car production line," *Advanced Robotics*, vol. 25, pp. 473–489, 2011.

[2] M. Mukadam, A. Borum, and T. Bretl, "Quasi-static manipulation of a planar elastic rod using multiple robotic grippers," in *IROS*, 2014, pp. 55–60.

[3] V. Viswanath, K. Shivakumar, J. Kerr, and coauthors, "Autonomously untangling long cables," in *Robotics: Science and Systems (RSS)*, 2022.

[4] R. C. Jackson and M. C. Cavusoglu, "Needle path planning for autonomous robotic surgical suturing," in *ICRA*, 2013, pp. 1669–1675.

[5] S. Javdani, S. Tandon, J. Tang, J. F. O'Brien, and P. Abbeel, "Modeling and perception of deformable one-dimensional objects," in *ICRA*, 2011, pp. 1607–1614.

[6] W. Wang, M. Bell, and D. Balkcom, "Towards arranging and tightening knots and unknots with fixtures," *IEEE Trans. on Automation Science and Engineering*, vol. 12, pp. 1318–1331, 2015.

[7] H. Wakamatsu, E. Arai, and S. Hirai, "Knotting/unknotting manipulation of deformable linear objects," *The Int. J. of Robotics Research*, vol. 25, no. 4, pp. 371–395, 2006.

[8] J. Till and D. Rucker, "Elastic stability of Cosserat rods and parallel continuum robots," *33(3) IEEE Trans. on Robotics*, pp. 1–16, 2017.

[9] O. Aghajanzadeh, M. A. J. Ramon, and coauthors, "Adaptive deformation control for elastic linear objects," *Frontiers in Robotics and AI*, vol. 9, pp. 1–13, Article 868459, 2022.

[10] P. Chang and T. Padir, "Model-based manipulation of linear flexible objects: Task automation in simulation and real world," in *IEEE/ASME Int. Conf. on Advanced Intelligent Mechatronics*, 2020, pp. 6–10.

[11] "IntelliMan – AI-powered manipulation system for advanced robotic service, manufacturing and prosthetics," European Union Horizon Project," https://intelliman-project.eu/, 2022-2026.

[12] "SoftEnable – towards soft fixture-based manipulation primitives in hazardous healthcare and food handling applications," European Union Horizon Project," https://softenable.eu/, 2022-2026.

[13] C. D. J. Zhu, A. Cherubini and coauthors, "Challenges and outlook in robotic manipulation of deformable objects," *IEEE Robotics & Automation Magazine*, pp. 2–12, 2022.

[14] "3rd workshop on representing and manipulating deformable objects," ICRA," https://deformable-workshop.github.io/icra2023/, 2023.

[15] "4th workshop on representing and manipulating deformable objects," ICRA," https://deformable-workshop.github.io/icra2024/, 2024.

[16] Z. Wang, S. Hirai, and S. Kawamura, "Challenges and opportunities in robotic food handling: A review," *Frontiers in Robotics and AI*, vol. 8, pp. 1–12, Article 789107, 2022.

[17] A. Love, *Mathematical Theory of Elasticity*. Dover, New York, 1944.

[18] H. Mochiyama, "Model validation of discretized spatial closed elastica," in *IROS*, 2016, pp. 5216–5223.

[19] H. Wakamatsu and S. Hirai, "Static modeling of linear object deformation based on differential geometry," *The Int. J. of Robotics Research*, vol. 23, no. 3, pp. 293–311, 2004.

[20] M. Moll and L. E. Kavraki, "Path planning for deformable linear objects," *IEEE Trans. on Robotics*, vol. 22, no. 4, p. 625–636, 2006.

[21] T. Bretl and Z. McCarthy, "Quasi-static manipulation of a Kirchhoff elastic rod based on geometric analysis of equilibrium configurations," *The Int, J. of Robotics Research*, vol. 33, no. 1, pp. 48–68, 2014.

[22] A. Sintov, S. Macenski, A. Borum, and T. Bretl, "Motion planning for dual-arm manipulation of elastic rods," *IEEE Robotics and Automation Letters*, vol. 5, no. 4, pp. 6065–6072, 2020.

[23] M. Yu, K. Lv, C. Wang, M. Tomizuka, and X. Li, "A coarse-to-fine framework for dual-arm manipulation of deformable linear objects with whole-body obstacle avoidance," in *ICRA*, 2023, pp. 10 153–10 159.

[24] A. Levin, E. Rimon, and A. Shapiro, "Steering flexible linear objects in planar environments by two robot hands using euler's elastica solutions," Jan 2025. [Online]. Available: https://arxiv.org/abs/2501.02874

[25] R. F. Hartl, S. P. Sethi, and R. G. Vickson, "A survey of the maximum principles for optimal control problems with state constraints," *SIAM Review*, vol. 37, no. 2, pp. 181–218, 1995.

[26] L. S. Pontryagin, V. G. Boltyanskii, R. V. Gamkrelidze, and E. F. Mishchenko, *The Mathematical Theory of Optimal Processes*. Interscience Publishers John Wiley & Sons, New York-London, 1962.

[27] V. Prasolov and Y. Solovyev, *Elliptic Functions and Elliptic Integrals*, AMS, Providence, RI, 1997.

[28] T. Sano and H. Wada, "Snap-buckling in asymmetrically constrained elastic strips," *Phys. Rev. E*, vol. 97, p. 013002, 2018.

[29] I. Gelfand and S. Fomin, *Calculus of Variations*. Englewood Cliffs, New Jersey: Moscow State University, Revised English Edition Translated and Edited by Richard A. Silverman, published in english by Prentice-Hall, INC., 1963.

[30] D. Liberzon, *Calculus of Variations and Optimal Control Theory*. New Jersey: Princeton University Press, 2012.

[31] Y. L. Sachkov, "Conjugate points in Euler's elastic problem," *J. of Dynamical and Control Systems*, vol. 14, pp. 409–439, 2008.

[32] M. Batista, "Elfun18 – a collection of MATLAB functions for the computation of elliptic integrals and jacobian elliptic functions of real arguments," *SoftwareX, http://www.sciencedirect.com/journal/softwarex*, vol. 10, pp. 1–10, 2019.

[33] R. L. Williams, "Baxter humanoid robot kinematics," https://academia.edu/35398090/Baxter_Kinematics, Academia.edu, 2025.

[34] D. Berenson, S. S. Srinivasa, D. Ferguson, and J. J. Kuffner, "Manipulation planning on constraint manifolds," in *ICRA*, 2009, pp. 625–632.

[35] A. Levin and I. Grinberg, "Flexible cable steering," ME, Technion," Online video: https://youtu.be/DDuveQGpR9M, 2025.